Title

Nanofibre optic force transducers with sub-piconewton resolution via near-field plasmon—dielectric interactions

Journal

Nature Photonics, 11(6)

ISSN

1749-4885

Authors

Huang, Qian

Lee, Joon

Arce, Fernando Teran

et al.

Publication Date

2017-06-01

DOI

10.1038/nphoton.2017.74

Peer reviewed

HHS Public Access

Author manuscript

Nat Photonics. Author manuscript; available in PMC 2018 March 22.

Published in final edited form as:

Nat Photonics. 2017 ; 11: 352–355. doi:10.1038/nphoton.2017.74.

Nanofibre optic force transducers with sub-piconewton resolution via near-field plasmon–dielectric interactions

Qian Huang[1,†], **Joon Lee**[2,†], **Fernando Teran Arce**[2,3,4,†,‡], **Ilsun Yoon**[1,‡], **Pavimol Angsantikul**[1], **Justin Liu**[2], **Yuesong Shi**[2], **Josh Villanueva**[1], **Soracha Thamphiwatana**[1], **Xuanyi Ma**[3], **Liangfang Zhang**[1,2,5], **Shaochen Chen**[1,2,3], **Ratnesh Lal**[2,3,4], and **Donald J. Sirbuly**[1,2,*]

[1]Department of NanoEngineering, University of California, San Diego, La Jolla, California 92093, USA

[2]Materials Science and Engineering, University of California, San Diego, La Jolla, California 92093, USA

[3]Department of Bioengineering, University of California, San Diego, La Jolla, California 92093, USA

[4]Department of Mechanical and Aerospace Engineering, University of California, San Diego, La Jolla, California 92093, USA

[5]Moores Cancer Center, University of California, San Diego, La Jolla, California 92093, USA

Abstract

Ultrasensitive nanomechanical instruments, including the atomic force microscope (AFM)[1–4] and optical and magnetic tweezers[5–8], have helped shed new light on the complex mechanical environments of biological processes. However, it is difficult to scale down the size of these instruments due to their feedback mechanisms[9], which, if overcome, would enable high-density nanomechanical probing inside materials. A variety of molecular force probes including mechanophores[10], quantum dots[11], fluorescent pairs[12,13] and molecular rotors[14–16] have been designed to measure intracellular stresses; however, fluorescence-based techniques can have short operating times due to photo-instability and it is still challenging to quantify the forces with high

*Correspondence and requests for materials should be addressed to D.J.S. dsirbuly@ucsd.edu.

†These authors contributed equally to this work.

‡Present addresses: Division of Translational and Regenerative Medicine, College of Medicine, and Department of Biomedical Engineering, University of Arizona, Tucson, Arizona 85721, USA (F.T.A.). Department of Chemistry, Chungnam National University, Daejeon 34134, Republic of Korea (I.Y.).

Author contributions

Q.H., I.Y. and D.J.S. designed the project. Q.H., J. Lee and Y.S. fabricated samples and ran the optical experiments. I.Y. and F.T.A. built the AFM-optical system. J. Lee, F.T.A. and Q.H. ran the AFM experiments. P.A. and S.T. prepared the bacteria solution. J. Liu and X.M. prepared the cell samples. Q.H. and D.J.S. wrote the manuscript. J. Lee, F.T.A., J.V., S.C., L.Z. and R.L. helped edit and revise the manuscript.

Supplementary information is available in the online version of the paper.

Competing financial interests

The authors declare no competing financial interests.

spatial and mechanical resolution. Here, we develop a compact nanofibre optic force transducer (NOFT) that utilizes strong near-field plasmon–dielectric interactions to measure local forces with a sensitivity of <200 fN. The NOFT system is tested by monitoring bacterial motion and heart-cell beating as well as detecting infrasound power in solution.

The design and working principle of the NOFT is shown in Fig. 1a. SnO_2 nanofibre waveguides (WGs)[17] were placed on a substrate (silica or quartz) and gold nanoparticles (~80 nm diameter) were directly attached to the bare nanofibre via electrostatic forces to serve as reference nanoparticles ($NP_{reference}$). The sensor nanoparticles (NP_{sensor}) were attached by covalently linking cystamine-functionalized NPs to a polyethylene glycol (PEG) monolayer grafted to the WG (Supplementary Section 1). The scattering intensity of NP_{sensor} is strongly dependent on the WG–NP separation distance. Therefore, to quantitatively read-out forces on NP_{sensor} via an optical signal, a link must be established between (1) the scattering intensity and polymer thickness and (2) the polymer thickness and the force applied on the nanoparticle. Both of these links can be achieved by initiating an accurate calibration model. We statistically measured a 0.55 ± 0.05 ratio of the average scattering intensities between NP_{sensor} and $NP_{reference}$ (Fig. 1b) and determined that the mechanical stiffness of the PEG films is stable up to two weeks when kept in phosphate-buffered saline (PBS) solution (Supplementary Fig. 1).

White defect emission is launched down the WG by exciting one end of it with a light source above the bandgap of SnO_2 (3.6 eV) (ref. 17). Since the position of the plasmonic nanoparticles can be optically tracked in the far-field with ångström-level spatial resolution[18], forces on the nanoparticles can be extracted by monitoring the scattering intensity, assuming the mechanical properties of the polymer cladding are well characterized. The force sensitivity of the NP_{sensor} can be calculated by multiplying the distance sensitivity ($D_{sensitivity}$) and the spring constant (k_{PEG}) of the PEG film. $D_{sensitivity}$ is determined by the minimum discernible intensity and the relationship between intensity and distance, such that $D_{sensitivity} = (\Delta\sigma/\mu)/S_{distance}$, where $\Delta\sigma/\mu$ is the change in the coefficient of variation from the average scattering intensity (μ) of NP_{sensor}, and $S_{distance}$ is the local slope of the scattering intensity versus WG–NP distance curve. As shown in Fig. 1c, the curves of σ/μ versus μ for both $NP_{reference}$ and NP_{sensor} follow similar trends indicating that there is no observable thermal-related vibration from NP_{sensor} on the polymer. This is likely due to the dense polymer brush underneath NP_{sensor} and an increased drag coefficient close to the surface[19,20]. From the noise level of these two curves, $\Delta\sigma/\mu$ is consistently centered at 0.005, independent of whether there is a PEG layer underneath or not.

An AFM integrated with an optical microscope was used to calibrate the force response of the NOFT. Due to the difficulty of reproducibly applying force directly on a NP_{sensor} with a bare AFM tip, which often caused the NP to dislodge from the polymer film (Supplementary Fig. 2), we simultaneously measured the optical signal from a single-NP-modified AFM tip (spring constant $k = 9.4$ pN nm^{-1}) and force–distance curves. Previous work has showed that the AFM tip does not influence the scattering intensity during interaction of the NP with the WG (Supplementary Fig. 3)[21]. As the modified tip approaches the WG, the scattering intensity increases, plateauing with larger intensity fluctuations when the polymer is fully

compressed (Fig. 1e and Supplementary Fig. 4). The increased modulation is likely caused by small sliding of the tip along the WG surface (contacting slightly different regions of the nanofibre)[22]. The force-scattering intensity versus time-retraction curve (latter 50 s in Fig. 1e) can be converted to force-scattering intensity versus distance (Fig. 1f) as the speed of the cantilever is known. During retraction of the AFM tip, we observed a 30% drop in the intensity (decay constant of 33 nm) from its maximum point within 10 nm, which corresponds to the thickness of the PEG monolayer in the force curve. We obtained an average PEG thickness of 15 ± 1 nm and a PEG chain density of 0.036 ± 0.006 chains nm^{-2} by fitting the force curve with the Alexander–de Gennes model for brush polymers[23,24] (Supplementary Section 2 and Supplementary Fig. 5). From the scattering intensity profile, a NP_{sensor} sitting on a 15-nm-thick PEG film corresponds to a 55% decrease in scattering intensity compared with $NP_{reference}$, agreeing well with the measured scattering intensity ratio in Fig. 1b. This result indicates that the NOFT platform detects forces prior to the AFM, and demonstrates that the AFM indentation experiments underestimate (10 nm) the real thickness of the PEG film (15 nm) underneath NP_{sensor}. From the scattering–distance relationship we extracted a value of 0.019 nm^{-1} for $S_{distance}$ and 2.6 Å for $D_{sensitivity}$ at a distance of 15 nm from the WG. We obtained a value of ~160 fN for the force sensitivity ($F_{sensitivity}$) using the Alexander–de Gennes model and evaluating the first derivative of the force at the contact point ($k_{PEG} = 6.3 \times 10^{-4}$ nN nm^{-1}).

To demonstrate the performance of the calibrated NOFT in quantifying forces[25], we placed NOFTs in a solution of *Helicobacter pylori* (*H. pylori*) bacteria (Fig. 2a and Supplementary Section 3). We recorded the scattering intensity of NP_{sensor} with and without bacteria (see Methods) and plotted the relationships of σ/μ versus μ (Fig. 2b). Because ultraviolet (UV) excitation can induce some fluorescence, causing a slight increase in background noise, we developed a statistical method to discriminate the background noise from the true signal. When the background noise δ is small compared with the signal, σ/μ increases linearly with respect to $1/\mu^2$ (Fig. 2c). The slopes of the lines reflect the noise level of the system, and the intercept with the vertical axis corresponds to the root mean square (r.m.s.) of the deformation depth ratio $\sqrt{(\Delta t^2)}$ (the ratio formed by the distance fluctuations Δx over the scattering decay constant (33 nm) of the nanoparticle) (Supplementary Section 4). When active bacteria are present, $\sqrt{(\Delta t^2)}$ increases by 0.016, which translates to a force of ~400 fN by the bacteria (a similar value to the propulsion force of a single bacterium[26,27]). The detected force is likely due to (i) the microflow forces induced by bacteria swimming in the vicinity of NP_{sensor}, and/or (ii) the interaction of bacteria with the PEG cladding, thus producing oscillations of NP_{sensor}. A direct collision between a bacterium and NP_{sensor} is unlikely to occur due to the small cross-section of NP_{sensor} (Supplementary Section 5). Accordingly, no binding of the bacteria to the NOFT was observed (Supplementary Fig. 6). To verify that the measured force originated from motion of the bacteria, and not Brownian forces, dead bacteria were tested, resulting in a similar optical response as bacteria-free experiments (Supplementary Fig. 7). These results were compared with AFM measurements (Supplementary Section 6 and Fig. 2d). The r.m.s. of the AFM cantilever deflection in a solution without bacteria was 0.55 Å (Fig. 2e), giving a r.m.s. force sensitivity of 2.2 ± 0.2 pN (k = 40 pN nm^{-1}). After adding bacteria, the induced force was approximately 10 pN (Fig. 2f). Interestingly, the calculated average stress on NP_{sensor} is four orders of magnitude

higher than on the AFM cantilever (Supplementary Section 7). This is likely due to the small size of the nanoparticle (which has a small drag coefficient) that doesn't filter as much of the higher-frequency signals as the bulk cantilever[28]. This demonstrates that the NOFT is capable of monitoring sub-piconewton forces from microorganisms in a dynamic environment.

We subsequently explored the ability of the NOFT to detect acoustic signatures from both micromechanical and biomechanical systems[29]. An AFM tip was employed to generate small acoustic oscillations near a NP_{sensor} by vertical modulation at low frequencies (Fig. 3a). The small applied forces (~300 pN) did not produce any measurable vibration of the WG (Supplementary Figs 8 and 9), but once the tip was moved close to NP_{sensor} (at a distance of ~500 nm), Fourier transforms of the scattering intensity resolved the oscillation frequencies of 1 and 2 Hz that were applied to the AFM cantilever (Fig. 3b). From these experiments, we estimate that the NOFT can detect sound pressure levels down to −30 dB in water (Supplementary Section 8). With this sensitivity, acoustic signatures from many different biomechanical systems could be detectable. To explore this, we placed a NOFT ~100 μm away from a small assembly of neonatal mouse cardiomyocytes (Fig. 3c, Methods and Supplementary Section 9) and resolved beating frequencies of 1–3 Hz from the cells[30] (Fig. 3d). We also observed that the cardiomyocytes stopped beating after about 30 min as the cell culture solution cooled down[31] (Supplementary Fig. 10). The large spread in beating frequency is anticipated (supported by results from optical imaging techniques) as a smaller cluster of cells does not have complete coherence and will show cycling variations from cell to cell. This demonstrates that the NOFT platform is versatile and could lead to *in vivo* stethoscopic applications.

In summary, we developed a novel NOFT platform that leverages the optical response of plasmonic nanoparticles attached to a compressible cladding embedded in the evanescent field of a nanofibre. We achieved ångström-level distance sensitivity and a force sensitivity of 160 fN. After fully calibrating the system, the NOFT was used to detect sub-piconewton forces from the swimming action of bacteria, and acoustic signatures from beating cardiomyocytes with a sensitivity of −30 dB. With the ability to tune the force and dynamic range via the mechanical response of the compressible cladding, detect forces from multiple nanoparticles on a single fibre, and with a geometry that can be inserted into small volumes, NOFT will become a valuable tool for biomechanical and intracellular studies.

Methods

Integrated AFM−optical set-up

AFM–optical measurements were done using a Dimension Hybrid XYZ scanner (Bruker) on a Zeiss Axiovert 135TV inverted light microscope (Fig. 1d). The AFM scanner was run by Nanoscope software 5.31R1 (Bruker) and has a scan range of 90 × 90 μm^2. The 325-nm line from a continuous-wave helium cadmium laser (~2 mW) was launched through a quartz slide underneath a WG at an angle of ~45° relative to the sample plane. The scattering intensities were collected through a 10× objective with a 600-nm short-pass filter and recorded by an EMCCD camera (Andor Technology).

Optical set-up for the measurement of bacteria motion force

After placing a SnO_2 nanofibre (via micromanipulation) across a silica trench, it was fixed to the substrate using polydimethylsiloxane (PDMS), and PEG was grafted on the suspended nanofibre. A cured PDMS ring was placed around the channel, forming a reservoir that could be filled with the bacteria solution or just the PBS solution. The bacteria concentration was held fixed at 1.65×10^7 c.f.u. ml^{-1} for all experiments. After covering the PDMS ring with a thin fused silica chip (~170 μm thickness), one end of nanofibre was excited by 325 nm UV light (~10 mW) at an angle of ~45° relative to the sample plane. The scattering intensity signals were collected through a 50× objective and recorded by an EMCCD camera (Andor Technology). The sampling frequency was ~66 Hz, and the recording period was ~15 s.

Optical set-up for the measurement of cell beating frequency

325-μm-thick PEG gels containing neonatal mouse cardiomyocytes in a GelMA hydrogel were placed in a microfluidic chamber containing NOFTs in the cell culture solution (74% DMEM Fluobrite, 25% M199 medium without phenol red, 0.5% penicillin/streptomycin solution (Gibco), 0.5% 1 M HEPES buffer). A similar excitation and collection set-up to the bacteria experiment was used to detect the beating frequency of the cardiomyocytes. The sampling frequency was ~19 Hz, and the recording period was ~52 s.

Data availability

The data that support the findings of this study are available from the corresponding author upon reasonable request.

Supplementary Material

Refer to Web version on PubMed Central for supplementary material.

Acknowledgments

The authors acknowledge X. Qu, W. Zhu, S. Ward and J. Friend for helpful discussions. This work was supported by the National Science Foundation (ECCS 1150952) and the University of California, Office of the President (UC-LFRP 12-LR-238415). Grant support from the California Institute of Regenerative Medicine (grant no. RT3-07899) and the National Institutes of Health (grant no. R01EB021857) to S.C. was greatly appreciated. A part of this project was supported by the National Institute on Aging of National Institutes of Health (grant AG028709). This work was performed in part at the San Diego Nanotechnology Infrastructure (SDNI) of UCSD, a member of the National Nanotechnology Coordinated Infrastructure, which is supported by the National Science Foundation (grant no. ECCS-1542148).

References

1. Zlatanova J, Lindsay SM, Leuba SH. Single molecule force spectroscopy in biology using the atomic force microscope. Prog Biophys Mol Biol. 2000; 74:37–61. [PubMed: 11106806]
2. Binnig G, Quate CF, Gerber C. Atomic force microscope. Phys Rev Lett. 1986; 56:930–933. [PubMed: 10033323]
3. Neuman KC, Nagy A. Single-molecule force spectroscopy: optical tweezers, magnetic tweezers and atomic force microscopy. Nat Methods. 2008; 5:491–505. [PubMed: 18511917]
4. Clausen-Schaumann H, Rief M, Tolksdorf C, Gaub HE. Mechanical stability of single DNA molecules. Biophys J. 2000; 78:1997–2007. [PubMed: 10733978]

5. Perkins TT. Optical traps for single molecule biophysics: a primer. Laser Photon Rev. 2009; 3:203–220.
6. Moffitt JR, Chemla YR, Smith SB, Bustamante C. Recent advances in optical tweezers. Annu Rev Biochem. 2008; 77:205–228. [PubMed: 18307407]
7. Strick TR, Allemand JF, Bensimon D, Bensimon A, Croquette V. The elasticity of a single supercoiled DNA molecule. Science. 1996; 271:1835–1837. [PubMed: 8596951]
8. Wang MD, et al. Force and velocity measured for single molecules of RNA polymerase. Science. 1998; 282:902–907. [PubMed: 9794753]
9. Sirbuly DJ, Friddle RW, Villanueva J, Huang Q. Nanomechanical force transducers for biomolecular and intracellular measurements: is there room to shrink and why do it? Rep Prog Phys. 2015; 78:024101. [PubMed: 25629797]
10. Hickenboth CR, et al. Biasing reaction pathways with mechanical force. Nature. 2007; 446:423–427. [PubMed: 17377579]
11. Choi CL, Koski KJ, Olson ACK, Alivisatos AP. Luminescent nanocrystal stress gauge. Proc Natl Acad Sci USA. 2010; 107:21306–21310. [PubMed: 21098301]
12. Grashoff C, et al. Measuring mechanical tension across vinculin reveals regulation of focal adhesion dynamics. Nature. 2010; 466:263–267. [PubMed: 20613844]
13. Meng F, Suchyna TM, Sachs F. A fluorescence energy transfer-based mechanical stress sensor for specific proteins *in situ*. FEBS J. 2008; 275:3072–3087. [PubMed: 18479457]
14. Iio T, Takahashi S, Sawada S. Fluorescent molecular rotor binding to actin. J Biochem. 1993; 113:196–199. [PubMed: 8468324]
15. Kung CE, Reed JK. Microviscosity measurements of phospholipid-bilayers using fluorescent dyes that undergo torsional relaxation. Biochemistry. 1986; 25:6114–6121.
16. Kuimova MK, et al. Imaging intracellular viscosity of a single cell during photoinduced cell death. Nat Chem. 2009; 1:69–73. [PubMed: 21378803]
17. Law M, et al. Nanoribbon waveguides for subwavelength photonics integration. Science. 2004; 305:1269–1273. [PubMed: 15333835]
18. Yoon I, et al. Nanofiber near-field light-matter interactions for enhanced detection of molecular level displacements and dynamics. Nano Lett. 2013; 13:1440–1445. [PubMed: 23517010]
19. Gittes F, Schmidt CF. Thermal noise limitations on micromechanical experiments. Eur Biophys J. 1998; 27:75–81.
20. Liu LL, Kheifets S, Ginis V, Capasso F. Subfemtonewton force spectroscopy at the thermal limit in liquids. Phys Rev Lett. 2016; 116:228001. [PubMed: 27314738]
21. Huang Q, et al. Gap controlled plasmon-dielectric coupling effects investigated with single nanoparticle-terminated atomic force microscope probes. Nanoscale. 2016; 8:17102–17107. [PubMed: 27714046]
22. Bhushan B. Nanotribology, nanomechanics and nanomaterials characterization. Phil Trans R Soc A. 2008; 366:1351–1381. [PubMed: 18156126]
23. Butt HJ, et al. Steric forces measured with the atomic force microscope at various temperatures. Langmuir. 1999; 15:2559–2565.
24. de Gennes PG. Polymers at an interface; a simplified view. Adv Colloid Interface Sci. 1987; 27:189–209.
25. Kirchner SR, et al. Direct optical monitoring of flow generated by bacterial flagellar rotation. Appl Phys Lett. 2014; 104:093701.
26. Chattopadhyay S, Moldovan R, Yeung C, Wu XL. Swimming efficiency of bacterium *Escherichia coli*. Proc Natl Acad Sci USA. 2006; 103:13712–13717. [PubMed: 16954194]
27. Constantino MA, Jabbarzadeh M, Fu HC, Bansil R. Helical and rod-shaped bacteria swim in helical trajectories with little additional propulsion from helical shape. Sci Adv. 2016; 2:e1601661. [PubMed: 28138539]
28. Gittes F, Schmidt CF. Signals and noise in micromechanical measurements. Methods Cell Biol. 1998; 55:129–156. [PubMed: 9352515]
29. Ohlinger A, Deak A, Lutich AA, Feldmann J. Optically trapped gold nanoparticle enables listening at the microscale. Phys Rev Lett. 2012; 108:018101. [PubMed: 22304294]

30. Shroff SG, Saner DR, Lal R. Dynamic micromechanical properties of cultured rat atrial myocytes measured by atomic-force microscopy. Am J Physiol Cell Physiol. 1995; 269:C286–C292.

31. Pelling AE, Sehati S, Gralla EB, Valentine JS, Gimzewski JK. Local nanomechanical motion of the cell wall of *Saccharomyces cerevisiae*. Science. 2004; 305:1147–1150. [PubMed: 15326353]

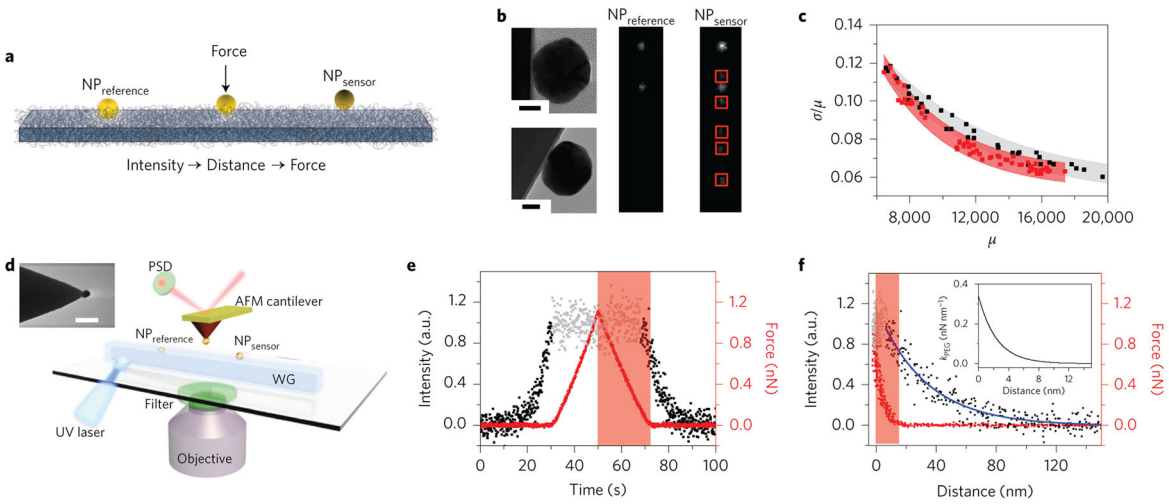

Figure 1. Nanofibre optic force transducer calibration

a, Schematic showing a $NP_{reference}$ directly on a nanofibre and a NP_{sensor} linked to a compressible PEG film grafted on the nanofibre. The scattering intensity of NP_{sensor} is directly related to its distance from the WG and the distance is strongly dependent on the applied force. **b**, Transmission electron microscopy images of a $NP_{reference}$ (top left) and NP_{sensor} (bottom left). Scale bars, 20 nm. Scattering images of two $NP_{reference}$ (middle) and several NP_{sensor} (red boxes) attached to a PEG film in the presence of the $NP_{reference}$ (right). **c**, The relationship between the coefficient of variation (σ/μ) and the average scattering intensity (μ) of $NP_{reference}$ (black squares) and NP_{sensor} (red squares). The grey and pink regions are the exponential decay fits to the experimental data with a change of 0.005. **d**, Scheme showing the simultaneous detection of nanoparticle scattering intensity, distance and force with a NP_{sensor} attached either to an AFM tip (calibration mode) or PEG film (sensing mode). Inset: scanning electron microscopy image of a single gold nanoparticle attached to an AFM tip. Scale bar, 200 nm. PSD, position sensitive detector. **e**, Relationship of scattering intensity (black dots) and force (red dots) with time. The grey dots indicate the optical saturation region when the PEG layer is fully compressed. **f**, Relationship of scattering intensity (black dots) and force (red dots) with respect to distance. The blue line is an exponential fit to the scattering intensity decay (decay constant takes on a value of 33 nm). Inset: relationship between the spring constant k_{PEG} and the distance fitted with the Alexander–de Gennes model. The contact section of the AFM retraction curve is highlighted with a red box in **e** and **f**.

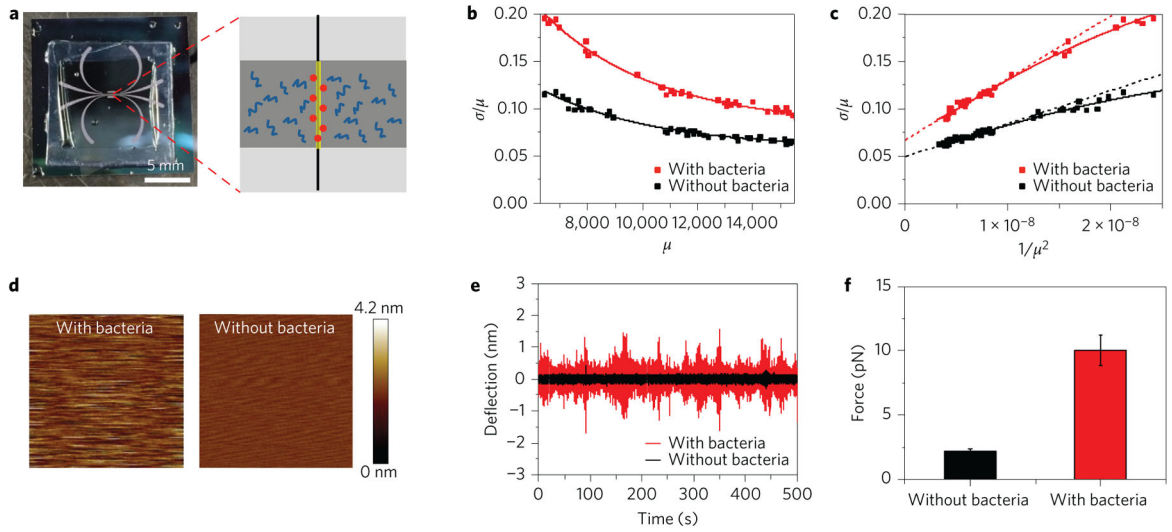

Figure 2. Detection of bacterial motile force

a, Left: photograph of a microfluidic chip that houses the NOFT device for detecting the force induced by *H. pylori* bacteria. Right: schematic showing a zoom-in of the NOFT sensor traversing a microfluidic channel. The bacteria (blue) periodically swim nearby the NP_{sensor} (red dots) causing optical modulations. **b**, Plot showing the relationship of the coefficient of variation (σ/μ) with respect to the average scattering intensity (μ) in PBS without bacteria and with active bacteria. Solid lines are a guide to the eye. **c**, Comparison of σ/μ with $1/\mu^2$ in PBS with and without bacteria. Solid lines are a guide to the eye. The dashed lines are linear fits to the data points below 1×10^{-8}. **d**, AFM deflection images obtained without feedback control in PBS with and without bacteria. **e**, Time-course of cantilever deflection in PBS with and without bacteria. **f**, Comparison of measured forces using AFM (deflection r.m.s. multiplied by the spring constant (k=40 pN nm^{-1})) in PBS with and without bacteria. The error bars are the standard deviations from ten different time-courses.

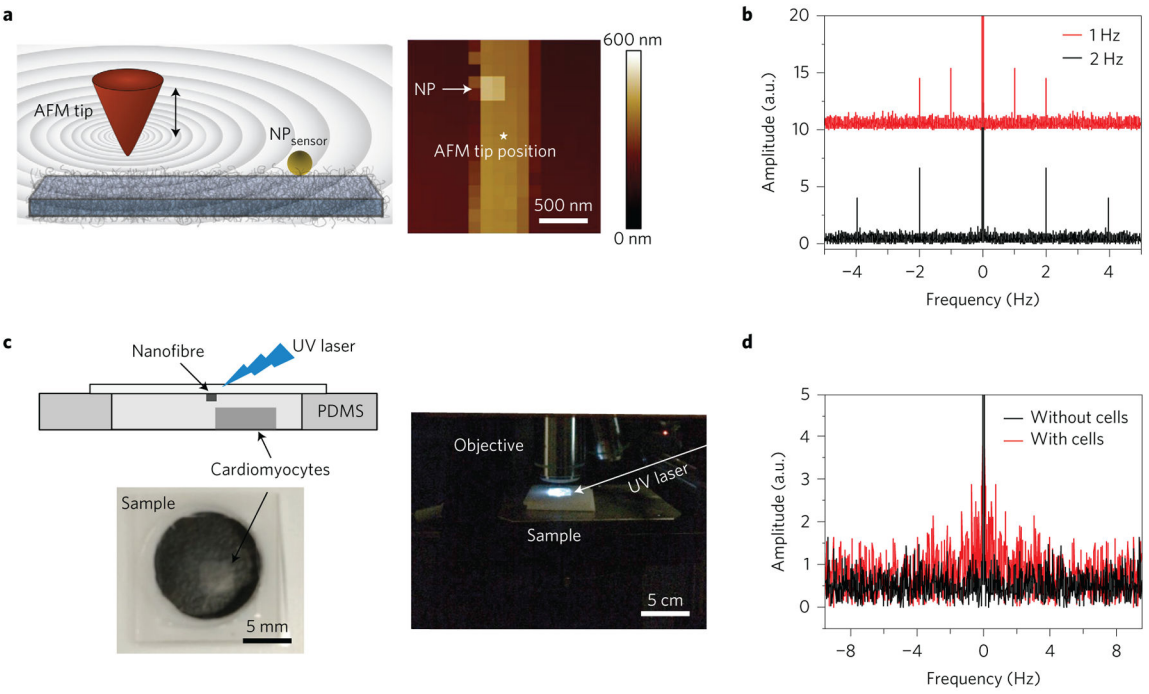

Figure 3. Acoustic frequency detection

a, Left: scheme showing an AFM tip acting (oscillating) as an acoustic source nearby a NP_{sensor}. Right: example of a force mapping image (~300 pN force) that was used to locate a NP_{sensor} and then the AFM tip was moved away to generate the acoustic wave. The double-headed arrow shows the movement of the AFM tip up and down to generate the acoustic wave. **b**, Fourier transformations of the NP_{sensor} scattering intensity after oscillating the AFM tip at two different frequencies (1 and 2 Hz). **c**, Top left: cross-sectional side view of the microfluidic chamber used to house the NOFT and cardiomyocyte cell cluster. The UV laser was focused through the quartz cover onto the NOFT without illuminating the cells, and scattering signals were collected back through a top-mounted microscope objective (pictured on the right). Bottom left: optical image of a sample containing the 3 mm× 3 mm× 250 μm cardiomyocyte cell cluster (black arrow) that was placed ~100 μm away from the NOFT in the microfluidic chamber. **d**, Fourier transforms taken from the end facet of the NOFT with and without cardiomyocytes.